Biomaterials 35 (2014) 814–824

Contents lists available at ScienceDirect

Biomaterials

journal homepage: www.elsevier.com/locate/biomaterials

Targeting the tumor-draining lymph node with adjuvanted nanoparticles reshapes the anti-tumor immune response

Susan N. Thomas [a,b], Efthymia Vokali [a], Amanda W. Lund [a,b], Jeffrey A. Hubbell [a,c,**], Melody A. Swartz [a,b,*]

[a] Institute of Bioengineering, École Polytechnique Fédérale de Lausanne (EPFL), Lausanne CH-1015, Switzerland
[b] Swiss Institute for Experimental Cancer Research (ISREC), École Polytechnique Fédérale de Lausanne (EPFL), Lausanne CH-1015, Switzerland
[c] Institute of Chemical Sciences and Engineering, École Polytechnique Fédérale de Lausanne (EPFL), Lausanne CH-1015, Switzerland

ARTICLE INFO

Article history:
Received 11 September 2013
Accepted 1 October 2013
Available online 18 October 2013

Keywords:
Sentinel lymph node
Tumor-draining lymph node
Drug delivery
Immunomodulation
Immunotherapy

ABSTRACT

Accumulating evidence implicates the tumor-draining lymph node (TDLN) in tumor-induced immune escape, as it drains regulatory molecules and leukocytes from the tumor microenvironment. We asked whether targeted delivery of adjuvant to the TDLN, presumably already bathed in tumor antigens, could promote anti-tumor immunity and hinder tumor growth. To this end, we used 30 nm polymeric nanoparticles (NPs) that effectively target dendritic cells (DCs, $CD11c^+$) within the lymph node (LN) after intradermal administration. These NPs accumulated within the TDLN when administered in the limb ipsilateral (i.l.) to the tumor or in the non-TDLN when administered in the contralateral (c.l.) limb. Incorporating the adjuvants CpG or paclitaxel into the NPs (CpG-NP and PXL-NP) induced DC maturation *in vitro*. When administered daily i.l. and thus targeting the TDLN of a B16–F10 melanoma, adjuvanted NPs induced DC maturation within the TDLN and reshaped the $CD4^+$ T cell distribution within the tumor towards a Th1 ($CXCR3^+$) phenotype. Importantly, this also led to an increase in the frequency of antigen-specific $CD8^+$ T cells within the tumor. This correlated with slowed tumor growth, in contrast to unhindered tumor growth after c.l. delivery of adjuvanted NPs (targeting a non-TDLN) or i.l. delivery of free adjuvant. CpG-NP treatment in the i.l. limb also was associated with an increase in $CD8^+/CD4^+$ T cell ratios and frequencies of activated ($CD25^+$) $CD8^+$ T cells within the TDLN whereas PXL-NP treatment reduced the frequency of regulatory T ($FoxP3^+$ $CD4^+$) cells in the TDLN. Together, these data implicate the TDLN as a delivery target for adjuvant therapy of solid tumors.

1. Introduction

Cancer immunotherapy aims to activate or enhance the patient's adaptive immune system to kill tumor cells with antigen specificity [1]. A number of strategies have been described, including delivering vaccines comprised of particular tumor antigens (or tumor lysate) together with a strong dendritic cell (DC) adjuvant such as CpG oligonucleotide or PolyI:C [2,3] or adoptive T cell therapy using the patient's own T cells that are transfected to express a chimeric antigen receptor against a tumor antigen [4]. However, tumors progress in part by exploiting a variety of immune evasion and suppression mechanisms, including attracting a highly suppressive cell and cytokine repertoire in the tumor stroma [5] and inducing anergy, exhaustion or deletion of tumor antigen-specific T cells [6–8], even when anti-tumor effector T cells are circulating systemically. For example, in patients with melanoma, DC maturation and activation within the sentinel or tumor-draining lymph node (TDLN) is inhibited [9], leading to less effective presentation of tumor antigens to prime anti-tumor cytotoxic T and T helper cells [10], even in the presence of highly immunogenic melanoma antigens [11–14]. Immunotherapies that either boost anti-tumor immunity or reverse tumor-induced immune suppression could be useful in managing the disease to compliment surgical debulking of the primary tumor.

* Corresponding author. Institute of Bioengineering, École Polytechnique Fédérale de Lausanne, Station 15, Lausanne CH-1015, Switzerland. Tel.: +41 021 693 9686; fax: +41 021 693 9670.
** Corresponding author. Department of Bioengineering, École Polytechnique Fédérale de Lausanne, Station 15, Lausanne CH-1015, Switzerland. Tel.: +41 021 693 9681; fax: +41 021 693 9685.
E-mail addresses: jeffrey.hubbell@epfl.ch (J.A. Hubbell), melody.swartz@epfl.ch (M.A. Swartz).

0142-9612
http://dx.doi.org/10.1016/j.biomaterials.2013.10.003

Treatment with immune cell-activating adjuvant without co-administered antigen is emerging as an alternative approach to promote adaptive immune responses against endogenously produced tumor antigens that might simultaneously boost global immune cell activation status and dampen immune regulation [15,16]. However, such immunotherapy with adjuvants has been largely explored via systemic administration schemes, or those targeting non-associated LNs, and has demonstrated some success in improving tumor outcome [1,15–18]. Efficacy may be limited partly because of the immune suppressed state of the TDLN, which can locally dampen anti-tumor effector T cells [16]. Thus, adjuvant immunotherapy might be most efficacious in alleviating tumor burden when provided to antigen presenting cells in close proximity to tumor antigen [16,19] or when targeted to tissues of particular immunological significance in tumor immunity and progression.

As an alternative to systemic immune activation, secondary lymphoid tissues such as the lymph nodes (LNs) have been proposed as intriguing sites for targeted immunotherapy [20]. Targeted delivery of antigen and adjuvant to LNs is increasingly being explored in vaccination [21–25] as well as transplantation-associated [26] immunotherapy, given the role of the LN in supporting adaptive immune cell priming responses [27]. DCs are present in high numbers in LNs relative to peripheral tissues such as the skin, suggesting that delivery of antigen and adjuvant to the LN might enhance vaccine efficiency. However, in addition to being a primary site for initiation of effector immune responses, the LN can be an important site for induction of immune tolerance, because regulatory T (T_{reg}) cells require the LN for activation [28–31]. Moreover, lymphatic transport of antigen from the periphery to the draining LN has been implicated in tolerance induction against peripherally encountered antigens [7], such as tissue-specific self-antigens being regionally drained to and through the TDLNs. As such, the LN is an intriguing therapeutic target for not only vaccination to induce prophylactic effector immunity as previously shown [21–24,32], but also for potentially modulating endogenous immune responses, in attempting to redirect tolerogenic pro-tumor immune responses.

In the context of solid tumors, the TDLN is thought to participate in disease progression on multiple levels. First, tumor lymphangiogenesis is associated with tumor progression [33,34], and LN metastasis is one of the primary clinical indicators of tumor progression at the time of tumor resection. Second, we recently reported that the TDLN and tumor-associated lymphangiogenesis play critical roles in promoting tumor immune escape [6,7]. Tumor-derived antigen and cytokine drainage might therefore prime not only the pre-metastatic niche but also an immune suppressive environment to promote tumor immune escape.

We hypothesized that given the presumption that the TDLNs are bathed in tumor-derived antigens, delivery of adjuvant alone may be adequate to help redirect pro-tumor responses, counting on tumor drainage to provide the antigen from endogenous sources. As such, adjuvant therapy to the TDLN could exploit the unique immunological crosstalk taking place between the TDLN and tumor, potentially reshaping the local suppressive cytokine and chemokine milieu towards an inflammatory environment while simultaneously harnessing draining tumor antigen to prime anti-tumor immunity or blunt pro-tumor immune escape pathways.

To test this hypothesis, we incorporated Toll-like receptor (TLR) ligands CpG oligonucleotide (a TLR-9 agonist [35]) or paclitaxel (PXL, a TLR-4 agonist [36]) in Pluronic-stabilized poly(propylene) sulfide (PPS)-core 30 nm nanoparticles (referred to as NPs, using this abbreviation to refer specifically to these nanoparticles) developed by our laboratory, which target immune cells resident within the draining LNs [21,37,38]. We explore how local adjuvant therapy can induce inflammation in the TDLN and reshape immune regulation in the tumor.

2. Materials and methods

2.1. Reagents

All reagents were obtained from Sigma–Aldrich (Büchs, Switzerland) unless stated otherwise. Cell culture grade media, serum, and antibiotics were from Life Technologies (Basel, Switzerland) unless otherwise noted.

2.2. Animals

C57BL/6 mice were purchased from Harlan. 6–8 wk old mice weighing 20 g were used for this study. All protocols were approved by the Veterinary Authority of the Canton Vaud according to Swiss law. Isofluorane was used as anesthesia. Mice were euthanized by CO_2 asphyxiation or cervical dislocation. Mice were injected intradermally with a bolus of 30–50 μL in the forelimb or intratumorally with 10 μL rhodamine-dextran. 0.5×10^6 cells were intradermally allografted in the left dorsal skin of the animal on day 0 and treatments were administered daily from day 4–9. Naïve or control (PBS) treated mice were used in each set of experiments. Tumor volume was calculated as the product of the width, length and height. Tumor volumes of naïve or control treated mice were used to normalize tumor volumes from different experiments. Three or more independent experiments were performed.

2.3. Cell culture

B16–F10 melanoma cells were cultured in Dubelcco's Modified Eagle Medium (DMEM) supplemented with 10% heat-inactivated fetal bovine serum (FBS) and penicillin/streptomycin (PS). Bone marrow-derived dendritic cells DCs were harvested from C57BL/6 mice as described [32] and used at day 8 after isolation. Briefly, femurs and tibiae were removed, the surrounding muscle tissue was detached and the bones were kept in RPMI 1640 media. Marrow was flushed out with RPMI 1640 using a syringe and passed through a 70 μm nylon cell strainer (BD Biosciences) to remove debris. Cells suspensions were centrifuged and resuspended in complete RPMI 1640 medium supplemented with penicillin-streptomycin, 50 mM beta-mercaptoethanol, FBS and sodium pyruvate, which was filtered through a vacuum driven disposable filtration system (MILLIPORE Stericup Express PLUS 0.22 μm, Millipore corporations, Massachusetts, USA). Cells were seeded in 100 mm diameter bacteriological petri dishes (BD Biosciences, San Jose, CA, US) at 5×10^6 cells per dish in 10 ml of complete RPMI medium containing 100 μl of recombinant mouse granulocyte-macrophage colony-stimulating factor (rmGM-CSF). At day 3 after isolation an additional 10 ml of complete medium containing rmGM-CSF were added to the plates. At day 6 after isolation, half of the culture supernatant was collected and centrifuged, and the cell pellet was resuspended in 10 ml of fresh complete medium containing rmGM-CSF and transferred back to the original plate. DCs on day 8 after isolation were transferred in 50 ml tubes, centrifuged and resuspended in fresh complete medium. Cells were plated in 96-well plates (BD Biosciences) at a density of $0.3–0.4 \times 10^6$ cells per well in 100 μl. 80 μl of fresh complete medium were added per well and plates were incubated at 37 °C until the treatments were prepared. Treatments were added at a volume of 20 μl.

2.4. In vivo fluid clearance and migration assay

10 μL 10,000 or 70,000 Da rhodamine-dextran (Sigma–Aldrich) was injected intratumorally. 30 min later, LNs i.l. and c.l. to the tumor were excised and homogenized in 500 l T-PER Tissue Protein Extraction Reagent (Pierce, Rockford, IL, USA) using Lysing Matrix D (MP Biomedicals, Illkirch, France) on a FastPrep-24 Automated Homogenizer (MP Biomedicals). Fluorescence was measured using a Safire2 TECAN plate reader (Tecan Group Ltd, Männedorf, Switzerland).

2.5. Immunofluorescence

30 min after rhodamine-dextran or AF488-NP injection, frozen LNs were cryosectioned (40 μm), counterstained with DAPI (Vector Laboratories, Burlingame, CA) and imaged using a LSM 510 confocal microscope (Carl Zeiss, Feldbach, Switzerland).

2.6. Nanoparticle synthesis and characterization

Pluronic-stabilized poly(propylene sulfide) (PPS) NPs with average diameters of 30 nm were synthesized by inverse emulsion polymerization as described previously [21,22,32,39,40]. Pluronic F-127 (a block copolymer of polyethylene glycol and polypropylene glycol terminated by hydroxyl groups) was used alone or in combination with carboxyl-terminated Pluronic derivatized as previously described [22,39,40]. Polymerization in the hydrophobic core results in PPS chains with a terminal thiolate, which can lead to stabilization of the core by intermolecular disulfide crosslinking [39]. However, since crosslinking cannot reach completion, remaining free sulfide groups on the NP surface were irreversibly capped by reaction with the alkylating reagent iodoacetamide. Alternatively, NP core thiols were reacted with a Dy488-meleimide 24 h at RT. Free dye was removed by dialysis against MilliQ water using 100,000 Da MWCO membranes. An absence of free dye was confirmed by high performance liquid chromatography (Waters, Montreux-

Chailly, Switzerland) using a Sepharose CL-6B column. NP suspensions were sterile-filtered and stored at 4C. The size of NPs was characterized by dynamic light scattering (DLS) in a Zetasizer nano-ZS with a modified zeta potential measurement cells (Malvern Instruments Ltd, Worcestershire, U.K.).

2.7. Pyridyl disulfide-NPs

Pyridyl disulfide-NPs were synthesized as previously described [23,24,40,41]. Briefly, to a NP suspension formed using 30% carboxylate Pluronic and 70% hydroxylate Pluronic, solid 2-(N-morpholino)ethanesulfonic acid was added to obtain a final concentration of 100 mM and the pH was adjusted to 4.0–4.5. Pyridyl disulfide cysteamine HCl salt, N-hydroxysulfosuccinimide sodium salt, and *N*-(3-dimethylaminopropyl)-*N′*-ethylcarbodiimide, all at an excess of 20 equivalents relative to the amount of carboxylate Pluronic, were added. Pyridyl disulfide cysteamine HCl salt was synthesized as previously described [40]. After reaction for 24 h, the solution was dialyzed against MilliQ water for at least 2 days to remove unreacted reagents using 100,000 Da MWCO membranes.

2.8. CpG conjugation of NPs

CpG-B 1826 thiophosphate (CpG) was obtained from Microsynth (Balgach, Switzerland). 20 nmoles CpG-SPO_3 was added to 1 ml pyridyl disulfide-NPs and reacted for 24 h at RT. CpG-conjugated NPs (CpG-NPs) were purified away from free CpG by gravity filtration on a Sepharose CL-6B column. Fractions containing NPs were identified using iodine staining and the CpG concentration was determined using Gel Red (Brunschwig, Basel, Switzerland).

2.9. PXL loading of NPs

PXL (Cat.number P-9600, MW 853.91 LC Laboratories, Woburn, MA USA) was dissolved at 5 mg/ml in tetrahydrofuran (THF). 20% by volume of this solution was added to 35 mg/ml NPs (aq) and immediately mixed by inversion for 5 min and subsequently spun at 16,000 g for 5 min. In order to determine the efficiency of PXL loading, the supernatant was collected after centrifugation and freeze dried, and the amount of PXL in the supernatant versus the pellet was measured by gel permeation chromatography (Waters). For experimentation, PXL-NPs (the supernatant after centrifugation) were dialyzed against MilliQ water with a 10,000 Da MWCO membrane using a dialysis cassette (Thermo Scientific, Rockford, IL, USA) overnight at RT in order to remove THF. The following day, the dialyzed PXL-NPs were recovered from dialysis, centrifuged, and supernatants stored at 4 °C until use.

2.10. Cell treatments

Free CpG, CpG-NPs, Ultra-pure LPS 01:11 B4 (Invivogen), and PXL-NPs were used to treat cells. Treatments were added at a volume of 20 μl. The CpG- and PXL-NP treatments were serially diluted with unloaded plain NPs. LPS and/or CpG, as well as PBS were used as positive and negative controls respectively. Cells were pulsed with the above mentioned treatments for 24 h.

2.11. Flow cytometry

After 24 h of stimulation, control non-treated and treated DCs were harvested and pellets were stained in order to analyze their phenotype by flow cytometry. Alternatively, lymphocytes were harvested from LNs and tumors from control or treated tumor-bearing mice by digestion with collagenase D (Roche Ltd., Mannhein, Germany) and tissue homogenization using 70 μm pore size strainers. Cell pellets were washed in HBSS containing 0.1% BSA (staining buffer) and centrifuged at 300 g for 1 min. Supernatants were decanted and cells stained with LD violet (Life Technologies, Carlsbad, CA) diluted in HBSS for 20 min. Cells were washed with staining buffer and monoclonal antibodies against mouse MHC-II, CD11c, CD86 and CD40, conjugated with FITC, PECy5, PECy5.5, AF647 or PE and appropriately diluted in staining buffer were added to cells and incubated for 30 min at 4 °C in the dark. Alternatively, the following anti-mouse antibodies were used for flow cytometry of harvested lymphocytes: CD45-APC, CD3e-FITC or CD3e-PerCPCy5.5, CD4-PECy7, CD8α-APC-Alexa 780, CD25-PE, CXCR3-APC, CD11c-Alexa 647, CD11b-PECy7, CD86-PE (all from eBioscience, San Diego, CA). Antibodies were prepared in HBSS/0.5% BSA and added to samples prior to incubation at 4 °C for 30 min in the dark. For detection of the Tyrosinase related protein-2 (Trp2) 180-188 H-2Kb MHCI peptide SVYDFFVWL, samples were stained with PE-conjugated SIINFEKL tetramer (Proimmune, Oxford, UK) diluted 1:10 in HBSS/0.5% BSA for 10 min at RT in the dark. Data was acquired in a Dako Cyan flow cytometer (Dako, Glostrup, Denmark) with compensation using either calibration beads (BD Biosciences, San Jose, CA) or single-stained cells. Data analysis was performed using FlowJo software (version 8.8, Ashland, OR).

2.12. Cytokine ELISAs

IL-12p40 and CXCL10 ELISAs (eBioscience) were performed on supernatants from DC stimulations according to the manufacturer's protocols.

2.13. Statistical analysis

Data are represented as the mean with the S.E.M. Statistics were calculated using Prism 5 software. Statistical significance was defined as $p < 0.05$ following one-way ANOVA and post-hoc analysis for dextran/NP drainage assays and immunological readouts or by Two-way ANOVA with matching for tumor growth comparisons. When normality tests failed, Kruskal–Wallis tests were performed. In drainage assays, $^{*}p < 0.05$, $^{**}p < 0.01$ and $^{***}p < 0.001$ with respect to contralateral limb or injection site as indicated. For immunological readouts and tumor growth comparisons, $^{*}p < 0.05$, $^{**}p < 0.01$ and $^{***}p < 0.001$ with respect to PBS control and $\dagger p < 0.05$, $\dagger\dagger p < 0.01$ and $\dagger\dagger\dagger p < 0.001$ with respect to the same treatment in the c.l. limb.

3. Results

3.1. Lymphatic drainage from tumor and ipsilateral limb to the tumor-draining lymph nodes

To evaluate the therapeutic utility of targeting the TDLN to reshape immune responses against a growing tumor, we used the B16–F10 model of melanoma, a well-described syngeneic and orthotopic mouse model that exhibits potent immune suppressive features [5,42]. We implanted tumors in the left dorsal skin near the shoulders (Fig. 1A) in order to focus tumor drainage to one side of the animal, thus creating TDLNs on the i.l. side and non-tumor-draining LNs (NTDLNs) on the c.l. side. Tumor lymphatic drainage tracked by intratumoral injection of rhodamine-dextran accumulated exclusively in the axillary and brachial LNs i.l. but not c.l. to the tumor (subsequently referred to as the TDLN and NTDLN, respectively) (Fig. 1B).

To target the TDLN without direct intratumoral injection, we sought to exploit the lymphatic capillary and vessel network that transports fluids, small molecules and cells away from the forelimbs to draining LNs (Fig. 1C). NPs that have been developed and extensively characterized by our laboratory [6,39,40] are sufficiently small and stealth to be quickly taken up into lymphatic vessels and transit to the draining lymph node after injection [21,37,38]. We found that NPs injected intradermally in the i.l., but not c.l., forelimb accumulated within both the axillary and brachial TDLNs (Fig. 1D, E). When injected in the c.l. forelimb, NPs accumulated almost exclusively in the NTDLNs (Fig. 1D). Importantly, therefore, this tumor model allowed us to test the effects of local TDLN immunomodulation without any direct effects of biomolecular delivery to the tumor, injecting into a co-draining region but not into the tumor itself.

3.2. Dendritic cell stimulatory activity of CpG conjugated NPs

An adjuvant of clinical interest is CpG oligodeoxynucleotide (CpG), a TLR9 agonist that demonstrates strong Th1 potentiating activity [35]. We have recently demonstrated that CpG delivery in conjunction with antigen-bearing NPs can dramatically enhance the frequency of antigen-specific $CD8^{+}$ T cells after intrapulmonary and intradermal administration [23,24]. Here, to chemically conjugate CpG to the NP surface, we utilized pyridyl disulfide-functionalized NPs, the synthesis [40] and use of which in conjugating thiol-containing protein antigens [23,24,41] have been previously reported. To conjugate CpG to the NPs, we reacted pydridyl disulfide-functionalized NPs synthesized with pydridyl disulfide-reactive 5′ thiophosphate-terminated CpG. This reaction yields CpG-conjugated NPs (CpG-NPs) with a reduction-sensitive covalent bond attaching the CpG to the Pluronic corona of the NPs (Fig. 2A). Size exclusion chromatography confirmed that CpG is bound to the NPs (Fig. 2B) and the CpG-NPs are ~30 nm in diameter by dynamic light scattering (Fig. 2C).

To confirm that CpG when conjugated to the NPs retains its immune stimulatory activity, we exposed them to murine bone marrow-derived immature DCs and measured their response. We

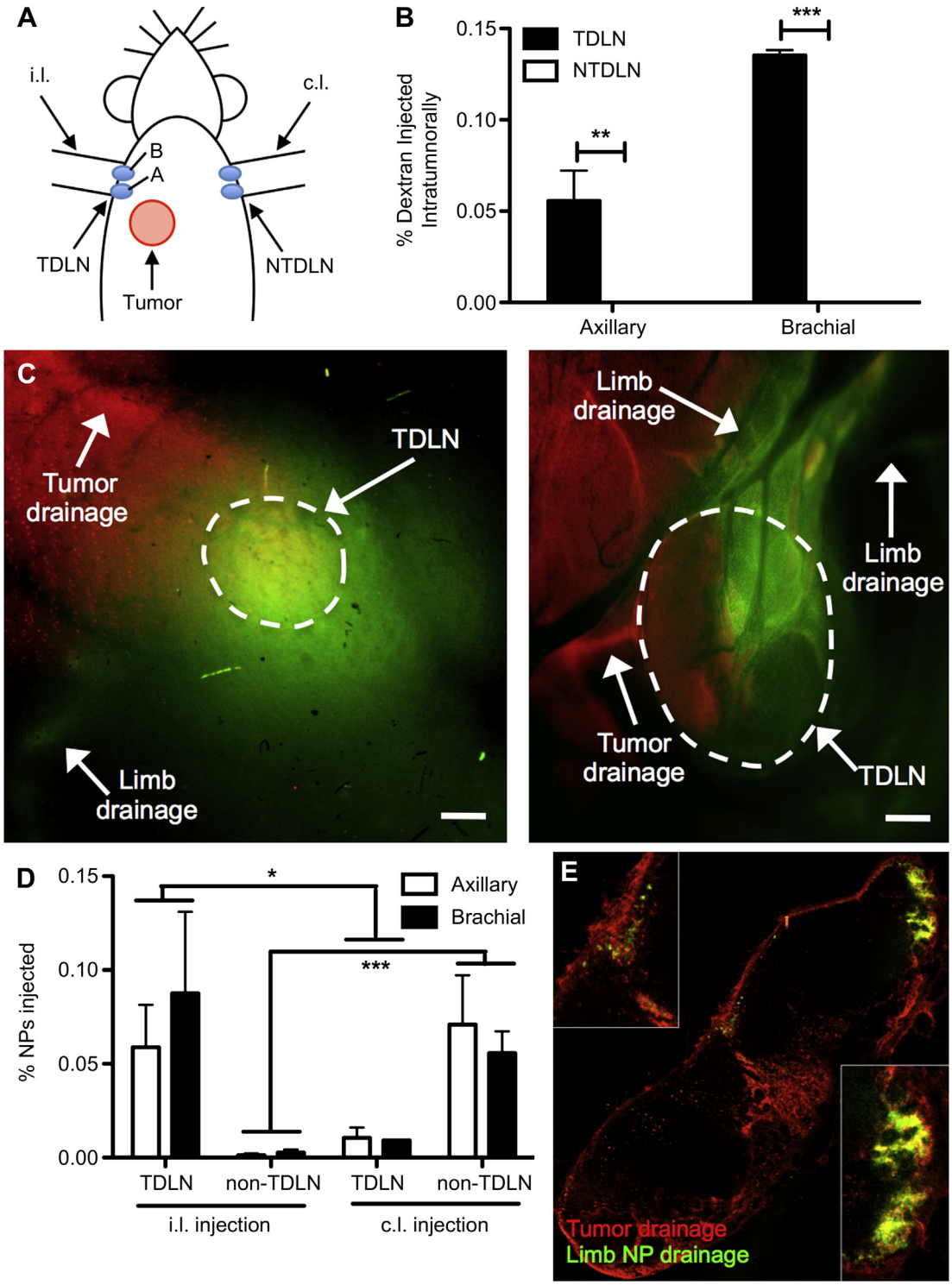

Fig. 1. Lymphatic-draining Pluronic-PPS NPs target the tumor-draining lymph node (TDLN) when injected in limb ipsilateral (i.l.) to tumor. (A) Location of tumor implantation relative to NP injection. (B–C) The i.l., but not contralateral (c.l.), axillary and brachial LNs drain fluorescent dextran injected into the tumor. Bar, 500 μm. (D–E) Lymphatic-draining NPs accumulate in the TDLN after injection i.l. but not c.l. to the tumor as measured by a (D) fluorescence plate reader or (E) fluorescence microscopy. Dextran, red. AF488-NPs, green. $^{*}p < 0.05$, $^{***}p < 0.001$ by ANOVA and posthoc Tukey's tests. Bar, 500 μm. (For interpretation of the references to colour in this figure legend, the reader is referred to the web version of this article.)

found that the maturation markers CD40, CD86 and MHCII increased in a dose-dependent fashion in response to CpG-NPs (Fig. 2D–E), as well as production of the inflammatory cytokines IL-12p40 and CXCL-10 (Fig. 2F). These data indicate that NP conjugation of CpG does not impair its immune stimulatory activity.

3.3. Tumor growth and infiltrating immune cell profile of LN and tumor in response to CpG-NP treatment of the TDLN

We next evaluated the efficacy of targeted CpG-NP delivery to the TDLN in influencing tumor immunity and growth. To this end, we implanted B16–F10 melanoma cells in the left shoulder dorsal

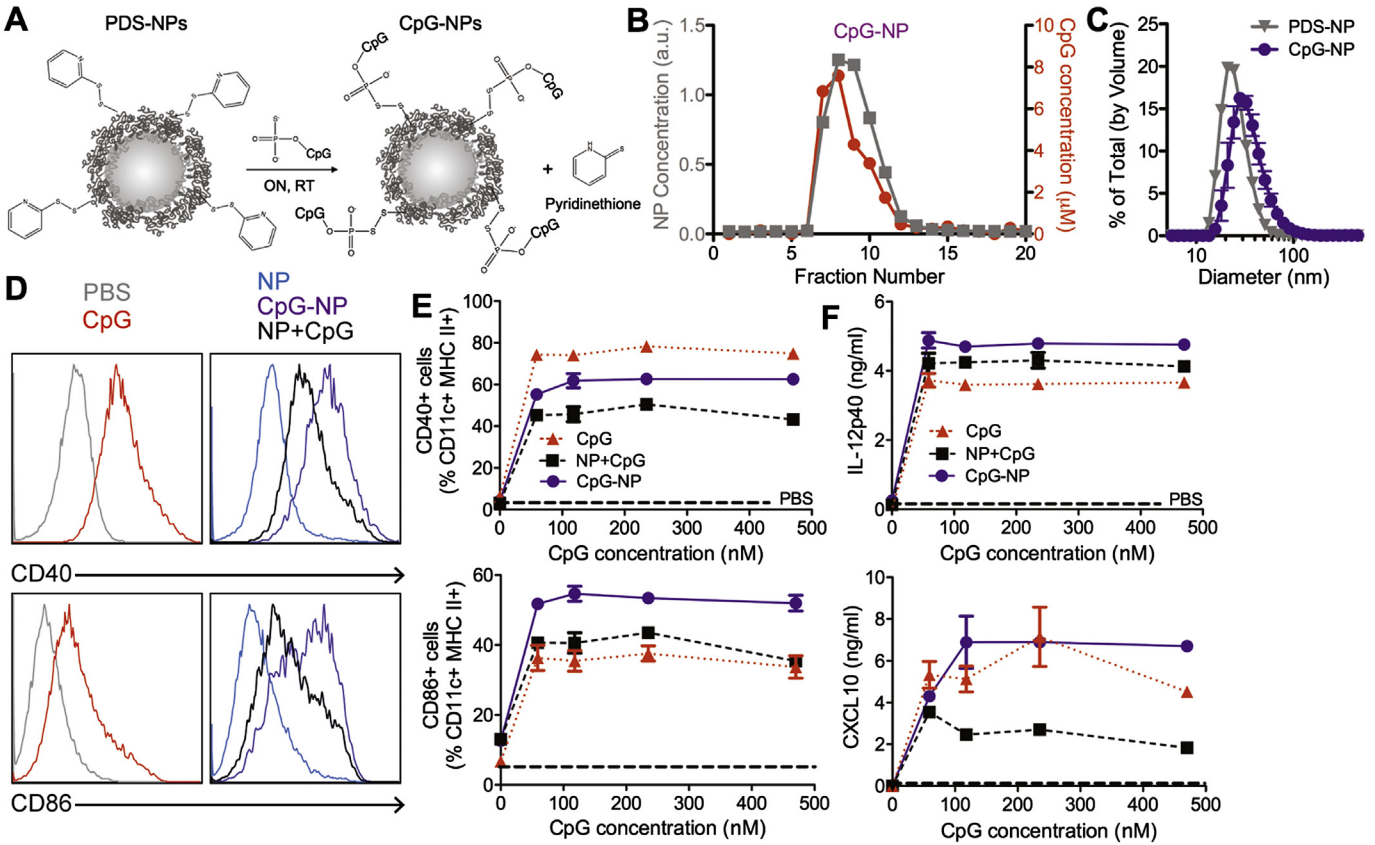

Fig. 2. CpG conjugated NP (CpG-NP) induce BMDC activation *in vitro*. (A) Schematic and (B) size exclusion chromatography demonstrating CpG conjugation to PDS NP using pyridyl disulfide conjugation chemistry. (C) Dynamic light scattering demonstrates homogeneous size distribution of ~ 30 nm of control (PDS)-NP and CpG-NP. (D) Representative flow cytometry histograms and (E) dose dependency of 24 h CpG-NP treatment on BMDC maturation. (F) IL-12p40 and CXCL-10 production with 24 h treatment of BMDCs with CpG-NP as measured by ELISA.

skin of C57BL/6 mice; after tumor establishment, we intradermally injected daily either CpG-NPs, free CpG mixed with the NPs, free CpG, or PBS in the limb i.l. or c.l. to the tumor (Fig. 3A). CpG-NP treatment of the i.l. limb was capable of slowing tumor growth relative to control treated mice (Fig. 3B), yet when CpG-NP was injected into the c.l. limb, no slowing of tumor growth was observed (Fig. 3B). Notably, treatment with free CpG mixed with NPs, free CpG or unmodified NPs had no effect on tumor growth (Fig. 3C), suggesting that CpG delivery to cells in the LN was more effective when the CpG was NP-conjugated.

Within the TDLN, a change in infiltrating immune cells was observed. In particular, the frequency of $CD11c^+$ cells was increased relative to saline-treated mice or mice treated with CpG-NP in the c.l. limb (Fig. 3D). Furthermore, the $CD11c^+$ cells were of a more mature phenotype as indicated by CD40 expression (Fig. 3E), although no differences were observed in CD86 expression (Fig. 3E). Small differences were observed in DC phenotype when considering CD11b or CD8a expression (Fig. 3F). In terms of the T cell composition within TDLNs targeted with CpG-NPs relative to naïve or PBS-treated controls, the ratio of $CD8^+$ to $CD4^+$ T cells was slightly increased in TDLNs of mice treated with CpG-NPs in the i.l. limb (Fig. 3G); more $CD8a^+$ T cells were found to be of an activated ($CD25^+$) phenotype (Fig. 3H), and a slightly higher frequency of $CXCR3^+$ $CD4^+$ T cells was observed (Fig. 3I). No changes in the frequencies of T_{reg} cells were observed, as

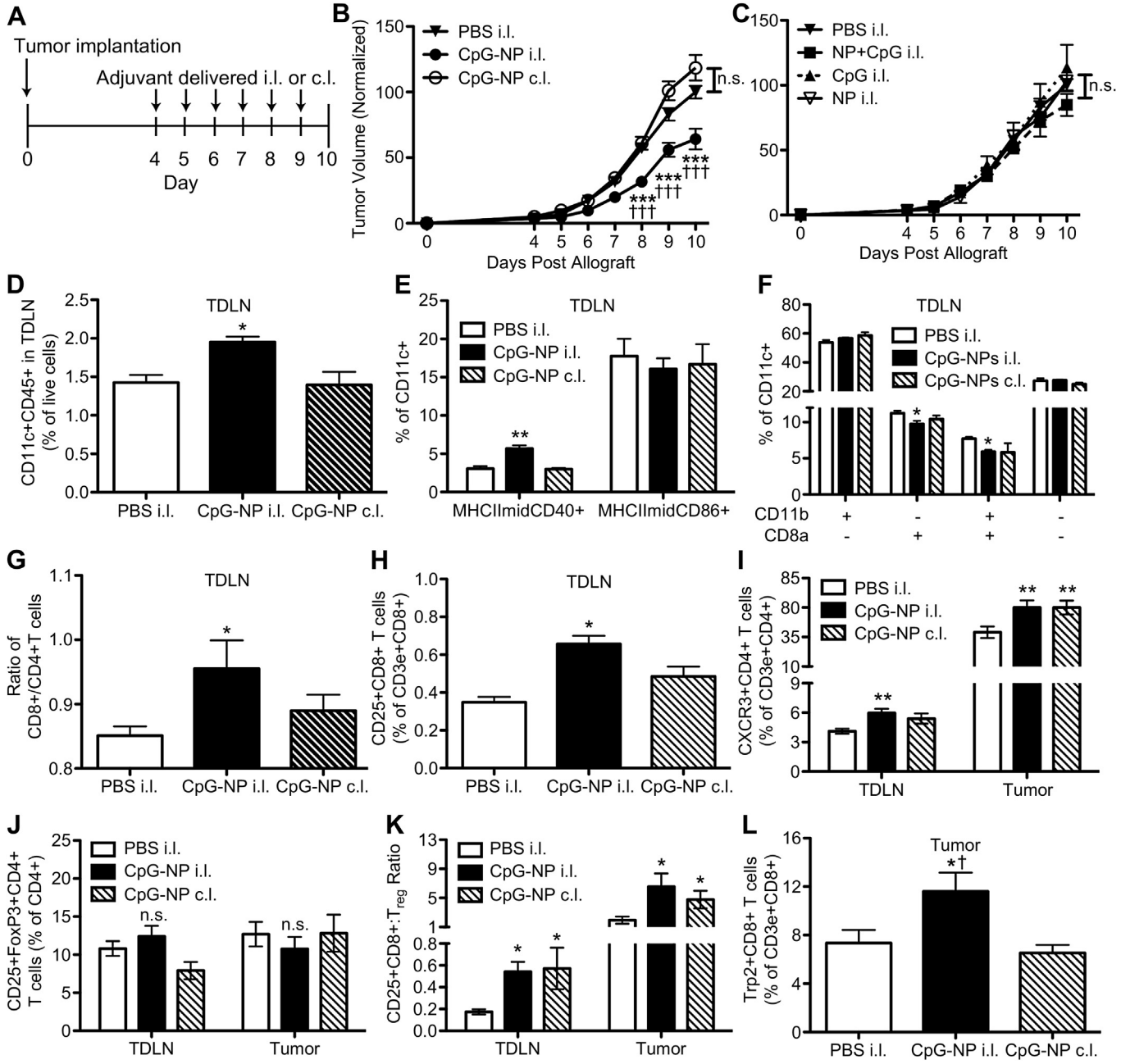

Fig. 3. CpG-NP treatment of B16–F10 melanoma TDLN slows tumor growth and changes infiltrating lymphocyte profile in TDLN and tumor. (A) Experimental treatment protocol. 5×10^5 B16–F10 cells were implanted into each mouse on day zero, and animals were treated daily from day 4–9. Treatment consisted of either saline delivered i.l., or CpG-NP with 3 μg CpG delivered into the i.l. or c.l. limb draining to the TDLN or NTDLN, respectively. (B) CpG-NP treatment of the LN ipsilateral (i.l.) but not contralateral (c.l.) to a B16–F10 tumor slows tumor growth. (C) Neither free CpG mixed with NP (NP + CpG), nor plain NP, nor free CpG effect B16–F10 melanoma tumor growth when applied to the limb i.l. to the tumor. (D–L) CpG-NP treatment of TDLN reshapes immune milieu within the TDLN (D–K) and tumor (I–L).

indicated by measurements of $CD25^+$ $FoxP3^+$ $CD4^+$ T_{reg} cells (Fig. 3J), in the TDLN and tumor. However, the frequencies of $CXCR3^+$ $CD4^+$ T cells in the tumor (Fig. 3I) and the ratio of activated ($CD25^+$) $CD8^+$ T cells to T_{reg} cells in the TDLN and tumor (Fig. 3K) increased with both i.l. and c.l. treatment. Notably, the frequencies of tumor-infiltrating, anti-tumor Trp2-specific $CD8a^+$ T cells (Fig. 3L) increased in mice treated with CpG-NPs in the limbs i.l. but not c.l. to the tumor. Together, these data suggest that co-drainage of CpG-NP into the TDLN, but not the NTDLN, led to immunomodulation that affected the immune response in the tumor, including the numbers of antigen-specific cytotoxic T cells infiltrating the tumor.

3.4. Dendritic cell stimulatory activity of PXL loaded NPs

Another adjuvant of interest is PXL, since it is already widely used in cancer chemotherapy. Here, rather than considering its usual role as an inhibitor of microtubule polymerization and thus proliferation in tumor cells, we rather consider its immune adjuvant role as an agonist for TLR4 [43] that has been explored to enhance cancer vaccine efficacy in lower doses [44]. As before, targeted delivery to the TDLN through co-drainage allowed us to evaluate immunomodulation in the TDLN independently of direct chemotherapy in the tumor.

Since PXL is hydrophobic, we incorporated it within the hydrophobic core of our NPs. PXL was loaded into the NPs at >95% loading efficiency, and release *in vitro* proceeded to 50% over a period of >50 h (Fig. 4A). Both PXL-loaded and mock THF (which uses the same solvent-loading process)-loaded NPs maintained a similar diameter (30 nm) relative to the untreated NPs (25 nm) as measured by dynamic light scattering (Fig. 4B). Both the PXL-NPs and THF-NPs were stable for >1 month when stored at 4 °C as determined by dynamic light scattering and gel permeation chromatography (data not shown).

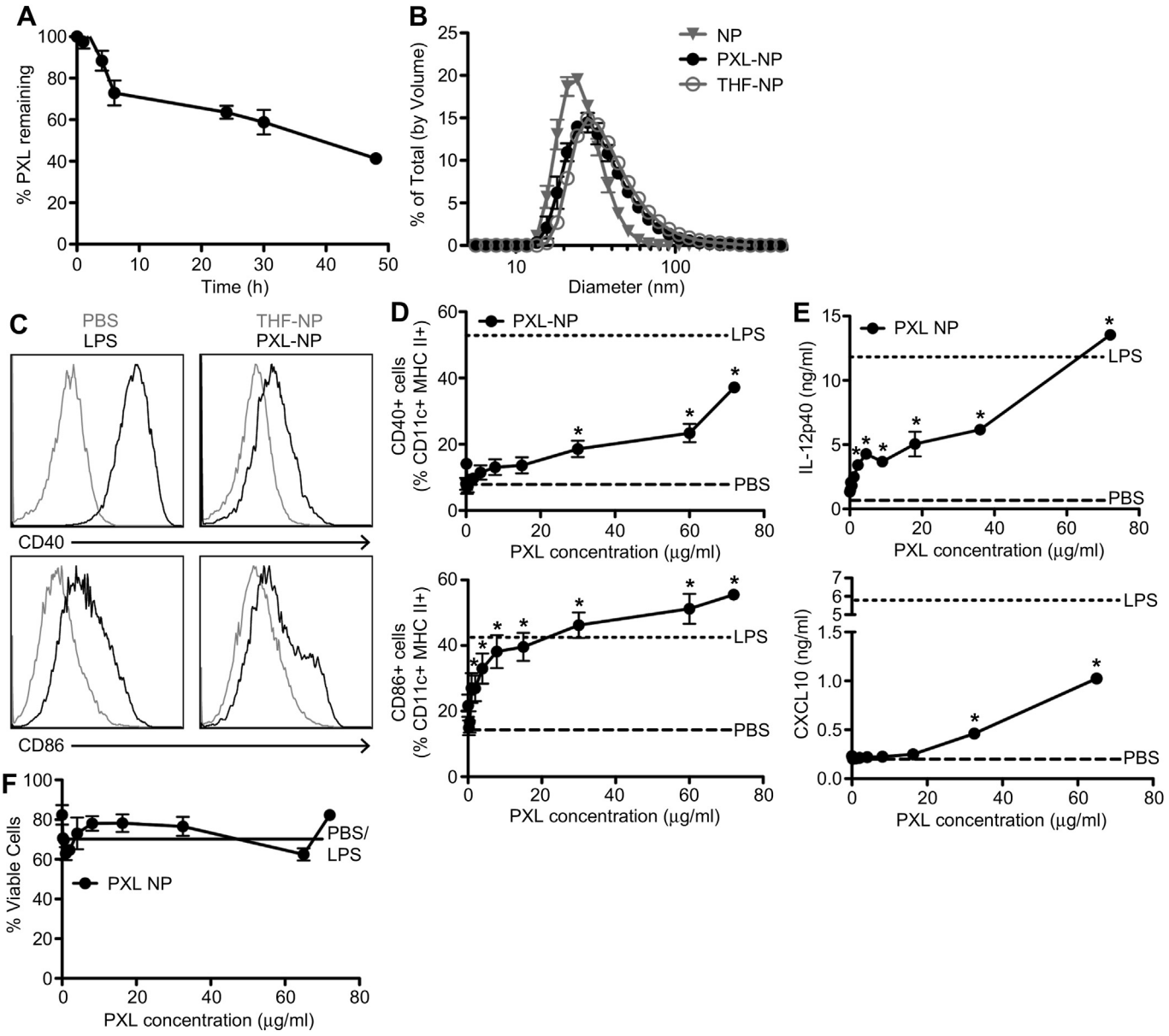

Fig. 4. PXL-loaded NP (PXL-NP) induce BMDC activation *in vitro*. (A) Release of PXL from NPs with dialysis. (B) NP diameter measured by dynamic light scattering shows NPs are monodisperse and ~30 nm in diameter when loaded with PXL dissolved in THF or plain THF (no PXL). (C) Representative flow cytometry histograms and (D) dose dependency of 24 h PXL-NP treatment on BMDC maturation. (E) IL-12p40 and CXCL10 production with 24 h treatment of BMDCs with PXL-NPs as measured by ELISA. (F) Cell viability after 24 h treatment of BMDCs with PXL-NPs. 0.5 μg/ml LPS used as positive control. 1000, 720, 72 μg/ml PXL used in (A), (B) and (C), respectively.

We next determined whether PXL encapsulated into our NPs would retain its immune stimulatory activity and induce DC maturation and cytokine production *in vitro,* as has been previously reported for the free drug [45]. When murine bone marrow-derived DCs were treated with PXL-NPs, we observed a dose-dependent increase in maturation above negative control (PBS) treatment in a manner analogous to positive control (LPS) treatment, as measured by CD40, CD86 and MHCII expression (Fig. 4C–D). Furthermore, we measured a PXL dose-dependent increase in inflammatory cytokine IL-12p40 and chemokine CXCL10 expression, above that induced by (negative control) PBS treatment and in a manner similar to that induced by (positive control) LPS treatment, with PXL-NP treatment (Fig. 4E). Moreover, PXL-NP treatment induced no cytotoxicity (Fig. 4F). These data indicate that PXL retains it immune stimulatory activity when encapsulated within NPs.

3.5. Tumor growth and infiltrating immune cell profile of LN and tumor in response to PXL-NP treatment of the TDLN

We evaluated whether targeting PXL-NP to the TDLN would influence the immune profile in the TDLN and tumor, and whether it would modulate tumor growth. We utilized the same B16–F10 model as described above, injecting mice in the i.l. or c.l. limb with PXL-NP or controls of unencapsulated PXL or unloaded NPs (Fig. 5A). We found that i.l. PXL-NP treatment was capable of

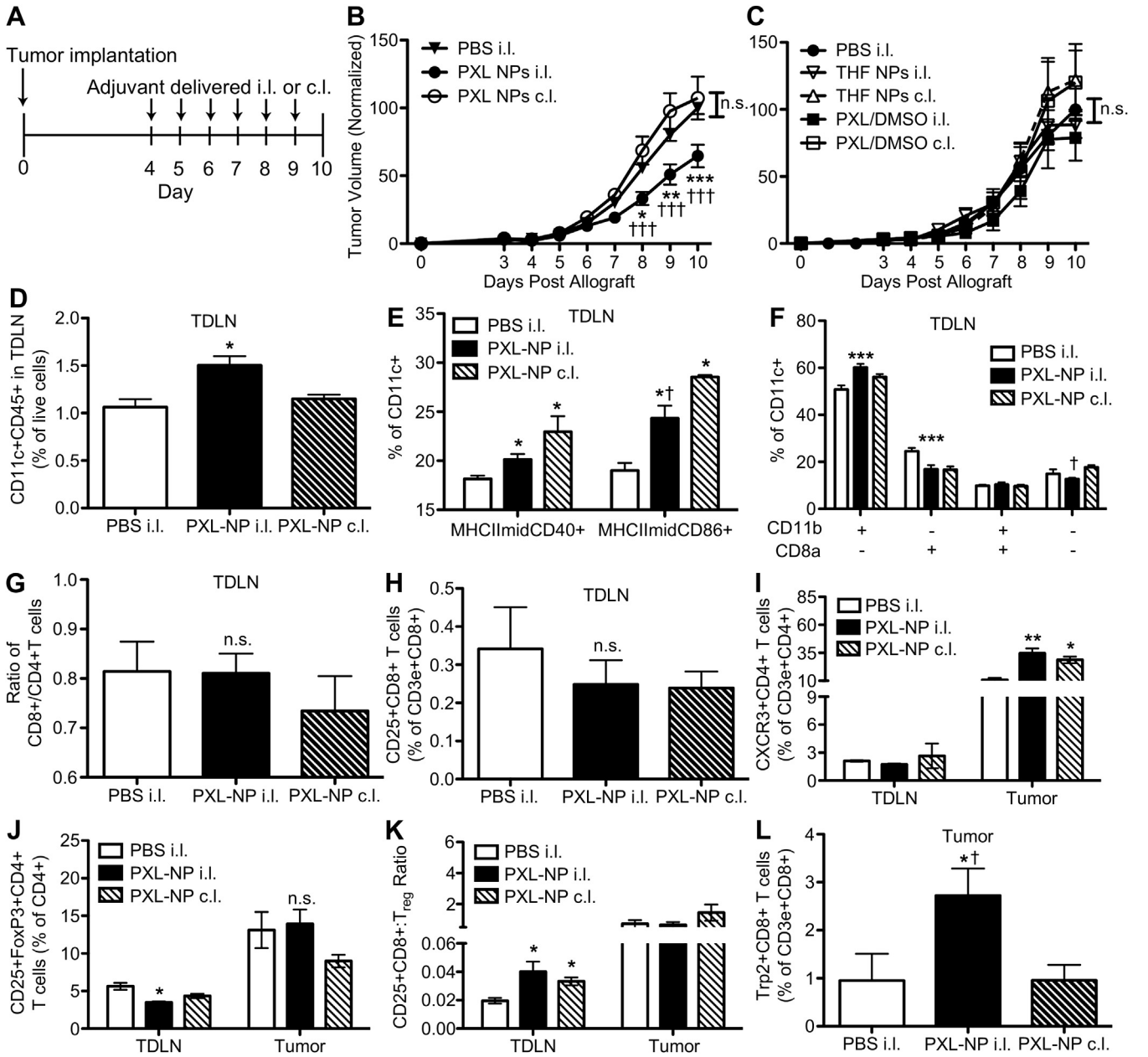

Fig. 5. PXL-NP treatment of B16–F10 melanoma TDLN slows tumor growth and changes infiltrating lymphocyte profile in TDLN and tumor. (A) Experimental treatment protocol. 5×10^5 B16–F10 cells were implanted into each mouse on day zero, and animals were treated daily from day 4–9. Treatment consisted of either saline delivered i.l., or PXL-NP with 35 μg PXL delivered into the i.l. or c.l. limb draining to the TDLN or NTDLN, respectively. (B) PXL-NP treatment of the LN ipsilateral (i.l.) but not contralateral (c.l.) to a B16–F10 tumor slows tumor growth. (C) Neither treatment with free PXL (in DMSO, PXL/DMSO) nor NPs without drug (THF-NPs) effect B16–F10 melanoma tumor growth. (D–L) PXL-NP treatment of TDLN reshapes immune milieu within the TDLN (D–K) and tumor (I–L).

slowing tumor growth relative to the control of PBS injection, however when PXL-NPs were injected in the c.l. limb, no diminution of tumor growth was observed (Fig. 5A). Moreover, free PXL (PXL/DMSO) and unloaded NPs (containing no drug, THF-NPs) had no effect on tumor growth (Fig. 5B–C). These data show that targeted, NP-mediated delivery of PXL to the TDLN alters tumor growth independently of direct action within the tumor.

As observed in experiments using CpG-NPs, changes in the immune cell profile within the TDLN and infiltration within the tumor were observed with PXL-NP treatment in the limb i.l. to the tumor. In particular, the frequency of $CD11c^+$ cells was increased in i.l. treated mice relative to c.l. treated mice (Fig. 5D), and activation of $CD11c^+$ cells was increased after both i.l. and c.l. treatment, with no differences in CD40 maturation levels between these two groups (Fig. 5E). Although there were elevations in $CD11b^+$ $CD8a^-$ $CD11c^+$ cell frequencies in the TDLN after i.l. but not c.l. treatment with PXL-NPs, differences between i.l. and c.l. treatment were not observed for $CD11b^-CD8a^+$ or $CD11b^+$ $CD8a^+$ $CD11c^+$ cells (Fig. 5F). However, unlike CpG-NP treated mice, the ratio of $CD8^+$ to $CD4^+$ T cells in the TDLN was unchanged, as were the frequencies of activated ($CD25^+$) $CD8^+$ T cells and $CXCR3^+$ $CD4^+$ T cells (Fig. 5G–I). The frequency of $CXCR3^+$ $CD4^+$ T cells infiltrating the tumor increased with both i.l. and c.l. PXL-NP treatment (Fig. 5H). Fewer T_{reg} cells ($CD25^+$ $FoxP3^+$ $CD4^+$) were observed in the TDLN after i.l. treatment (Fig. 5J), resulting in an increase in the $CD25^+$ $CD8^+$ to T_{reg} cell ratio in the TDLN (Fig. 5K). Most notably, in the tumor, i.l. but not c.l. PXL-NP treatment increased the frequency of anti-tumor Trp2-specific $CD8a^+$ T cells (Fig. 5L), correlating with the reduction in tumor growth for this group.

4. Discussion

The TDLN plays a specialized role in malignant disease progression, distinct from that of non-tumor associated LNs during normal immune surveillance. For example, while intranodal tumor challenge leads to tumor regression, primary extralymphatic tumors can rapidly anergize T cells in TDLNs [46]. However, immunopotentiation of the TDLN, via inhibition of TGF-β-mediated immunosuppression as one example, can augment anti-tumor immunity [47], implicating TDLN-targeted immunotherapy as a potential means by which to redirect tumor-associated immune suppression.

Herein, we explore the use of nanotechnology for tumor immunotherapy, but rather than using an immunization scheme, we implement NP-mediated delivery of TLR agonist adjuvants to the TDLN as a means to boost immune activation against tumor antigen *in situ*. Our hypothesis was that TDLN-targeted adjuvant therapy might effectively reshape the TDLN immune microenvironment and bias T cell priming against endogenously produced co-draining tumor antigen towards an effector type. Using two chemically and biologically distinct TLR agonists, we demonstrate that targeted delivery of adjuvant to the TDLN slows tumor growth (Figs. 3 and 5). In line with clinical observations of sentinel LN DC maturation status and composition correlating with sentinel LN metastasis [48], decreased tumor growth achieved by adjuvant-NP treatment of the i.l. forelimb was associated with recruitment, maturation and subtype redistribution of DCs within the TDLN (Fig. 3D–F, Fig. 5D–F) resulting in increased frequencies of $CXCR3^+$ $CD4^+$ T cells within the tumor (Figs. 3I and 5I). Moreover, tumor antigen ($Trp2^+$)-reactive $CD8^+$ $CD3e^+$ (Fig. 3L, Fig. 5L) T cell frequencies in the tumor were enhanced only with TDLN but not NTDLN adjuvant-NP treatment. Our data suggest that promoting $CD11c^+$ cell maturation by TLR activation within LNs bathed in draining tumor antigen can promote Th1-biased immunity that can exert effector function against the tumor.

Although NP-mediated delivery of both CpG and PXL TLR ligand adjuvants to TDLNs slowed tumor growth, the relative contribution of enhanced immune activation versus disfavored immune tolerance diverged. With CpG-NP but not PXL-NP treatment of the i.l. forelimb, Th1-biasing ($CXCR3^+$) $CD4^+$ and activated ($CD25^+$) $CD8a^+$ T cell frequencies increased within the TDLN (Fig. 3G–I), as did $CD8^+$:$CD4^+$ T cell ratio, which has been shown to correlate with decreased lymph node metastasis in human papillomavirus-induced cervical cancer [49] and survival in metastatic melanoma patients receiving chemotherapy [50]. Conversely, PXL-NP treatment, but not CpG-NP, treatment in the i.l. forelimb instead induced changes in the T_{reg} compartment in the TDLN (Fig. 5J). The cumulative affect resulted in both adjuvant-NP treatments inducing higher ratios of $CD25^+$ $CD8^+$ cells to T_{reg} cells within the TDLN (Figs. 3K and 5K). Indeed, T_{reg} cell frequencies and T_{reg}/Th17 ratios within TDLNs correlate with colorectal cancer diagnosis [51] as well as gastric cancer stage [52]. Hence, TDLN-targeted treatment with adjuvant might be capable of modulating both the generation of effector responses and blunting tumor-induced regulatory responses.

CpG is an adjuvant of significant clinical interest but has demonstrated limited clinical efficacy as a monotherapy [53]. Our results, which demonstrate that targeted NP-mediated CpG delivery to tissues co-draining tumor antigen, as opposed to a non-targeted approach, slows disease progression (Fig. 3B–C), suggests that conventional systemic administration schemes may limit CpG's potential efficacy, but that alternative administration approaches, in particular those that target it at bioactive doses to tissues co-draining tumor antigen, might remedy this. Indeed, recent clinical observations of increased DC activation [54] and melanoma tumor antigen-specific $CD8^+$ T cells [55] in sentinel LNs with preoperative perilesional dermal administration of B-class CpG in melanoma patients are consistent with this concept as well as the reported the efficacy of C-class, although not B-class, CpG administration in TDLN, but not via intravenous or intraperitoneal treatment, in reducing breast cancer tumor growth [56].

Most TLR ligands, including those recently approved for clinical use in vaccine applications, including lipid A analogs and squalene [57], are hydrophobic [58] and thus challenging to formulate for administration. As a model for demonstrating the utility of biomaterials-based formulations to deliver hydrophobic drugs to the TDLN for immunotherapy applications, we used PXL, a drug better known for its chemotherapeutic activity than its TLR4 agonist activity [43]. TDLN-targeted PXL chemotherapy is of interest as a means to manage recurrent disease within the sentinel LNs [59]. Moreover, taxane chemotherapy enhances cancer vaccine efficacy [44], suggesting PXL's immune modulatory activity might be harnessed for TDLN-targeted immunotherapy applications. Here, at sub-chemotherapeutic doses, we demonstrate strong immune activation within the TDLN by PXL-NP treatment in the i.l. limb. These results underscore the utility of biomaterials engineering strategies in tumor immunotherapy, localizing doses to specific lymphoid tissue targets.

5. Conclusions

We have demonstrated the utility of a nanobiotechnology-based approach to deliver immunomodulatory adjuvants to the TDLN to exploit the unique immunological crosstalk taking place between the tumor and the TDLN, which is bathed in both tumor antigens and suppressive tumor-derived cytokines. With TDLN-targed adjuvant therapy, we could reshape the local immune microenvironment to promote tumor antigen-specific effector immune responses. Reduced tumor growth required adjuvant delivery to the TDLN, since treatment of NTDLNs had no effect on tumor growth or

anti-tumor immune responses. Together, these data implicate the TDLN as a promising target lymphoid tissue for adjuvant therapy of solid tumors and suggest that lymphatic-targeting nanoparticle technology can be used to reformulate TLR agonists for use in adjuvant therapy applications.

Acknowledgments

The authors are grateful to André van der Vlies for advice as well as Patricia Corthésy-Henrioud, Didier Foretay, Miriella Pasquier and Vladanka Topalovic for technical assistance.

References

[1] Mellman I, Coukos G, Dranoff G. Cancer immunotherapy comes of age. Nature 2011;480:480–9.
[2] Wu A, Oh S, Gharagozlou S, Vedi RN, Ericson K, Low WC, et al. In vivo vaccination with tumor cell lysate plus CpG oligodeoxynucleotides eradicates murine glioblastoma. J Immunother 2007;30:789–97.
[3] Azuma M, Ebihara T, Oshiumi H, Matsumoto M, Seya T. Cross-priming for antitumor CTL induced by soluble Ag + polyI: C depends on the TICAM-1 pathway in mouse CD11c(+)/CD8alpha(+) dendritic cells. Oncoimmunology 2012;1:581–92.
[4] Kalos M, Levine BL, Porter DL, Katz S, Grupp SA, Bagg A, et al. T cells with chimeric antigen receptors have potent antitumor effects and can establish memory in patients with advanced leukemia. Sci Transl Med 2011;3. 95ra73.
[5] Shields JD, Kourtis IC, Tomei AA, Roberts JM, Swartz MA. Induction of lymphoidlike stroma and immune escape by tumors that express the chemokine CCL21. Science 2010;328:749–52.
[6] Swartz MA, Hirosue S, Hubbell JA. Engineering approaches to Immunotherapy. Sci Transl Med 2012;4. 148rv9.
[7] Lund AW, Duraes FV, Hirosue S, Raghaven V, Nembrini C, Thomas SN, et al. Tumor VEGF-C promotes immune tolerance and tumor antigen cross-presentation by lymphatics. Cell Rep 2012;1:191–9.
[8] Baitsch L, Baumgaertner P, Devêvre E, Raghav SK, Legat A, Barba L, et al. Exhaustion of tumor-specific CD8⁺ T cells in metastases from melanoma patients. J Clin Invest 2011;121:2350–60.
[9] Cochran AJ, Morton DL, Stern S, Lana AM, Essner R, Wen DR. Sentinel lymph nodes show profound downregulation of antigen-presenting cells of the paracortex: implications for tumor biology and treatment. Mod Pathol 2001;14:604–8.
[10] Pinzon-Charry A, Maxwell T, Lopez JA. Dendritic cell dysfunction in cancer: a mechanism for immunosuppression. Immunol Cell Biol 2005;83:451–61.
[11] Yamshchikov GV, Barnd DL, Eastham S, Galavotti H, Patterson JW, Deacon DH, et al. Evaluation of peptide vaccine immunogenicity in draining lymph nodes and peripheral blood of melanoma patients. Int J Cancer 2001;92:703–11.
[12] Banchereau J, Palucka AK, Dhodapkar M, Burkeholder S, Taquet N, Rolland A, et al. Immune and clinical responses in patients with metastatic melanoma to CD34(+) progenitor-derived dendritic cell vaccine. Cancer Res 2001;61:6451–8.
[13] Romero P, Dunbar PR, Valmori D, Pittet M, Ogg GS, Rimoldi D, et al. Ex vivo staining of metastatic lymph nodes by class I major histocompatibility complex tetramers reveals high numbers of antigen-experienced tumor-specific cytolytic T lymphocytes. J Exp Med 1998;188:1641–50.
[14] Jarmalavicius S, Welte Y, Walden P. High immunogenicity of the human leukocyte antigen peptidomes of melanoma tumor cells. J Biol Chem 2012;287:33401–11.
[15] Weigel BJ, Rodeberg DA, Krieg AM, Blazar BR. CpG oligodeoxynucleotides potentiate the antitumor effects of chemotherapy or tumor resection in an orthotopic murine model of rhabdomyosarcoma. Clin Cancer Res 2003;9:3105–14.
[16] Nierkens S, den Brok MH, Roelofsen T, Wagenaars JA, Figdor CG, Ruers TJ, et al. Route of administration of the TLR9 agonist CpG critically determines the efficacy of cancer immunotherapy in mice. PloS One 2009;4:e8368.
[17] Schlom J. Therapeutic cancer vaccines: current status and moving forward. J Natl Cancer Inst 2012;104:599–613.
[18] Kirkwood JM, Butterfield LH, Tarhini AA, Zarour H, Kalinski P, Ferrone S. Immunotherapy of cancer in 2012. CA Cancer J Clin 2012;62:309–35.
[19] Heckelsmiller K, Rall K, Beck S, Schlamp A, Seiderer J, Jahrsdorfer B, et al. Peritumoral CpG DNA elicits a coordinated response of CD8 T cells and innate effectors to cure established tumors in a murine colon carcinoma model. J Immunol 2002;169:3892–9.
[20] Hubbell JA, Thomas SN, Swartz MA. Materials engineering for immunomodulation. Nature 2009;462:449–60.
[21] Reddy ST, van der Vlies AJ, Simeoni E, Angeli V, Randolph GJ, O'Neil CP, et al. Exploiting lymphatic transport and complement activation in nanoparticle vaccines. Nature Biotechnol 2007;25:1159–64.
[22] Thomas SN, van der Vlies AJ, O'Neil CP, Reddy ST, Yu SS, Giorgio TD, et al. Engineering complement activation on polypropylene sulfide vaccine nanoparticles. Biomaterials 2011;32:2194–203.
[23] Ballester M, Nembrini C, Dhar N, de Titta A, de Piano C, Pasquier M, et al. Nanoparticle conjugation and pulmonary delivery enhance the protective efficacy of Ag85B and CpG against tuberculosis. Vaccine 2011;29:6959–66.
[24] Nembrini C, Stano A, Dane KY, Ballester M, van der Vlies AJ, Marsland BJ, et al. Nanoparticle conjugation of antigen enhances cytotoxic T-cell responses in pulmonary vaccination. Proc Natl Acad Sci U S A 2011;108:E989–97.
[25] Jewell CM, Lopez SC, Irvine DJ. In situ engineering of the lymph node microenvironment via intranodal injection of adjuvant-releasing polymer particles. Proc Natl Acad Sci U S A 2011;108:15745–50.
[26] Dane KY, Nembrini C, Tomei AA, Eby JK, O'Neil CP, Velluto D, et al. Nano-sized drug-loaded micelles deliver payload to lymph node immune cells and prolong allograft survival. J Control Release 2011;156:154–60.
[27] Randolph GJ, Angeli V, Swartz MA. Dendritic-cell trafficking to lymph nodes through lymphatic vessels. Nat Rev Immunol 2005;5:617–28.
[28] Forster R, Davalos-Misslitz AC, Rot A. CCR7 and its ligands: balancing immunity and tolerance. Nat Rev Immunol 2008;8:362–71.
[29] Schneider MA, Meingassner JG, Lipp M, Moore HD, Rot A. CCR7 is required for the in vivo function of CD4⁺ CD25⁺ regulatory T cells. J Exp Med 2007;204:735–45.
[30] Menning A, Hopken UE, Siegmund K, Lipp M, Hamann A, Huehn J. Distinctive role of CCR7 in migration and functional activity of naive- and effector/memory-like Treg subsets. Eur J Immunol 2007;37:1575–83.
[31] Ochando JC, Yopp AC, Yang Y, Garin A, Li Y, Boros P, et al. Lymph node occupancy is required for the peripheral development of alloantigen-specific Foxp3⁺ regulatory T cells. J Immunol 2005;174:6993–7005.
[32] Hirosue S, Kourtis IC, van der Vlies AJ, Hubbell JA, Swartz MA. Antigen delivery to dendritic cells by poly(propylene sulfide) nanoparticles with disulfide conjugated peptides: cross-presentation and T cell activation. Vaccine 2010;28:7897–906.
[33] Tammela T, Alitalo K. Lymphangiogenesis: molecular mechanisms and future promise. Cell 2010;140:460–76.
[34] Varney ML, Singh S, Backora M, Chen Z, Singh RK. Lymphangiogenesis and anti-tumor immune responses. Curr Mol Med 2009;9:694–701.
[35] Klinman DM. Immunotherapeutic uses of CpG oligodeoxynucleotides. Nat Rev Immunol 2004;4:249–58.
[36] Byrd-Leifer CA, Block EF, Takeda K, Akira S, Ding A. The role of MyD88 and TLR4 in the LPS-mimetic activity of Taxol. Eur J Immunol 2001;31:2448–57.
[37] Reddy ST, Rehor A, Schmoekel HG, Hubbell JA, Swartz MA. In vivo targeting of dendritic cells in lymph nodes with poly(propylene sulfide) nanoparticles. J Control Release 2006;112:26–34.
[38] Kourtis IC, Hirosue S, de Titta A, Kontos S, Stegmann T, Hubbell JA, et al. Peripherally administered nanoparticles target monocytic myeloid cells, secondary lymphoid organs and tumors in mice. PloS One 2013;8:e61646.
[39] Rehor A, Hubbell JA, Tirelli N. Oxidation-sensitive polymeric nanoparticles. Langmuir 2005;21:411–7.
[40] van der Vlies AJ, O'Neil CP, Hasegawa U, Hammond N, Hubbell JA. Synthesis of pyridyl disulfide-functionalized nanoparticles for conjugating thiol-containing small molecules, peptides, and proteins. Bioconjug Chem 2010;21:653–62.
[41] Stano A, van der Vlies AJ, Martino MM, Swartz MA, Hubbell JA, Simeoni E. PPS nanoparticles as versatile delivery system to induce systemic and broad mucosal immunity after intranasal administration. Vaccine 2011;29:804–12.
[42] Mattarollo SR, Steegh K, Li M, Duret H, Foong Ngiow S, Smyth MJ. Transient Foxp3(+) regulatory T-cell depletion enhances therapeutic anticancer vaccination targeting the immune-stimulatory properties of NKT cells. Immunol Cell Biol 2013;91:105–14.
[43] Kawasaki K, Akashi S, Shimazu R, Yoshida T, Miyake K, Nishijima M. Mouse toll-like receptor 4.MD-2 complex mediates lipopolysaccharide-mimetic signal transduction by Taxol. J Biol Chem 2000;275:2251–4.
[44] Garnett CT, Schlom J, Hodge JW. Combination of docetaxel and recombinant vaccine enhances T-cell responses and antitumor activity: effects of docetaxel on immune enhancement. Clin Cancer Res 2008;14:3536–44.
[45] Perera PY, Mayadas TN, Takeuchi O, Akira S, Zaks-Zilberman M, Goyert SM, et al. CD11b/CD18 acts in concert with CD14 and Toll-like receptor (TLR) 4 to elicit full lipopolysaccharide and taxol-inducible gene expression. J Immunol 2001;166:574–81.
[46] Preynat-Seauve O, Contassot E, Schuler P, Piguet V, French LE, Huard B. Extralymphatic tumors prepare draining lymph nodes to invasion via a T-cell cross-tolerance process. Cancer Res 2007;67:5009–16.
[47] Fujita T, Teramoto K, Ozaki Y, Hanaoka J, Tezuka N, Itoh Y, et al. Inhibition of transforming growth factor-beta-mediated immunosuppression in tumor-draining lymph nodes augments antitumor responses by various immunologic cell types. Cancer Res 2009;69:5142–50.
[48] Mansfield AS, Heikkila P, von Smitten K, Vakkila J, Leidenius M. Metastasis to sentinel lymph nodes in breast cancer is associated with maturation arrest of dendritic cells and poor co-localization of dendritic cells and CD8+ T cells. Virchows Arch 2011;459:391–8.
[49] Piersma SJ, Jordanova ES, van Poelgeest MI, Kwappenberg KM, van der Hulst JM, Drijfhout JW, et al. High number of intraepithelial CD8⁺ tumor-infiltrating lymphocytes is associated with the absence of lymph node metastases in patients with large early-stage cervical cancer. Cancer Res 2007;67:354–61.
[50] Hernberg M, Muhonen T, Turunen JP, Hahka-Kemppinen M, Pyrhonen S. The CD4⁺/CD8⁺ ratio as a prognostic factor in patients with metastatic melanoma receiving chemoimmunotherapy. J Clin Oncol 1996;14:1690–6.

[51] Deng L, Zhang H, Luan Y, Zhang J, Xing Q, Dong S, et al. Accumulation of foxp3$^+$ T regulatory cells in draining lymph nodes correlates with disease progression and immune suppression in colorectal cancer patients. Clin Cancer Res 2010;16:4105–12.
[52] Maruyama T, Kono K, Mizukami Y, Kawaguchi Y, Mimura K, Watanabe M, et al. Distribution of Th17 cells and FoxP3(+) regulatory T cells in tumor-infiltrating lymphocytes, tumor-draining lymph nodes and peripheral blood lymphocytes in patients with gastric cancer. Cancer Sci 2010;101:1947–54.
[53] Pashenkov M, Goess G, Wagner C, Hormann M, Jandl T, Moser A, et al. Phase II trial of a toll-like receptor 9-activating oligonucleotide in patients with metastatic melanoma. J Clin Oncol 2006;24:5716–24.
[54] Molenkamp BG, van Leeuwen PA, Meijer S, Sluijter BJ, Wijnands PG, Baars A, et al. Intradermal CpG-B activates both plasmacytoid and myeloid dendritic cells in the sentinel lymph node of melanoma patients. Clin Cancer Res 2007;13:2961–9.
[55] Molenkamp BG, Sluijter BJ, van Leeuwen PA, Santegoets SJ, Meijer S, Wijnands PG, et al. Local administration of PF-3512676 CpG-B instigates tumor-specific CD8$^+$ T-cell reactivity in melanoma patients. Clin Cancer Res 2008;14:4532–42.
[56] Yang L, Sun L, Wu X, Wang L, Wei H, Wan M, et al. Therapeutic injection of C-class CpG ODN in draining lymph node area induces potent activation of immune cells and rejection of established breast cancer in mice. Clin Immunol 2009;131:426–37.
[57] Tefit JN, Serra V. Outlining novel cellular adjuvant products for therapeutic vaccines against cancer. Expert Rev Vaccines 2011;10:1207–20.
[58] Seong SY, Matzinger P. Hydrophobicity: an ancient damage-associated molecular pattern that initiates innate immune responses. Nat Rev Immunol 2004;4:469–78.
[59] Khullar OV, Griset AP, Gibbs-Strauss SL, Chirieac LR, Zubris KA, Frangioni JV, et al. Nanoparticle migration and delivery of Paclitaxel to regional lymph nodes in a large animal model. J Am Coll Surg 2012;214:328–37.